Low-Reynolds-number swimming in viscous two-phase fluids

Jian Du,[1] James P. Keener,[1,2] Robert D. Guy,[3] and Aaron L. Fogelson[1,2]

[1]*Department of Mathematics, University of Utah, Salt Lake City, Utah 84112, USA*
[2]*Department of Bioengineering, University of Utah, Salt Lake City, Utah 84112, USA*
[3]*Department of Mathematics, University of California Davis, Davis, California 95616, USA*

The fluid media surrounding many microorganisms are often mixtures of multiple materials with very different physical properties. The composition and rheology of the mixture may strongly affect the related locomotive behaviors. We study the classical Taylor's swimming sheet problem within a two-fluid model, which consists of two intermixed viscous fluids with different viscosities, with both numerical experiments and analysis. Our results indicate that both the swimming speed and efficiency may be decreased substantially relative to those for a single-phase fluid.

PACS number(s): 47.63.Gd, 47.55.−t, 87.85.gj

I. INTRODUCTION

Locomotion of microorganisms at low Reynolds number occurs in numerous biological processes, from the propulsion of *Escherichia coli* toward more favorable regions within the intestine [1] to the motion of spermatozoa through mucus in the female reproductive tract [2]. Swimming in a Stokesian Newtonian fluid has been extensively studied and the underlying physics is well understood. See Ref. [3] for a review of low-Reynolds-number locomotion. Many biological fluids such as mucus are mixtures of water and polymers that are not appropriately described as Newtonian fluids. Recently, there have been many theoretical studies on locomotion in complex fluids [4–11].

Asymptotic analyses of infinitely long swimmers in a viscoelastic fluid showed that swimming is hindered by the addition of elastic stresses [5,6]. However, numerical simulation of finite-length swimmers in a viscoelastic fluid showed that under some conditions, the swimming speed may be enhanced [9]. It was shown that swimming though a Brinkman medium [8] results in enhanced swimming speeds.

For some complex materials, such as gels, there may be relative motion between the polymer network and the water, and then describing the material as a single continuous medium is inappropriate. The two-fluid model is a widely used approach to describe gel mechanics, where both network and solvent coexist at each point of space and each phase is modeled as a continuum with its own velocity field and constitutive law [12,13]. The classical problem of the swimming infinite sheet was recently analyzed using the two-fluid model in the case where the polymer network is modeled as an elastic or viscoelastic solid [10,11].

In this paper, we study the swimming of an infinite sheet within a two-fluid mixture, in which both the network and solvent are described as viscous Newtonian fluids. Our aim is to provide a theoretical understanding of how the composition and rheology of a mixture of two viscous fluids can have a profound effect on the swimming speed. Our work is relevant for understanding these effects, e.g., in a colloidal suspension (*E. coli* moving through milk) or for a polymeric solution for which the viscoelastic relaxation time is sufficiently short compared to the beating period of the swimmer.

We develop an extension of the immersed boundary method [14] to the two-fluid model to study aspects of the problem that are beyond the reach of asymptotic analysis alone. Using both numerical simulations and perturbation methods, we show that swimming in a viscous two-fluid mixture is always slower and less efficient than swimming in a single viscous fluid and that the composition of the mixture significantly affects the swimming speed.

This paper is the third of which we are aware that looks at the classic Taylor problem of an infinite undulating sheet in the context of a mixture of two materials. The others [10,11] examine swimming in a medium consisting of a mixture of a Newtonian fluid and an elastic [10] or viscoelastic [11] solid. While relative motion between the materials plays a role in these studies, both take the solid volume fraction to be vanishingly small and take the fluid to be incompressible. Depending on the boundary conditions imposed on the fluid at the undulating sheet, these studies report that either (visco-)elasticity of the medium always reduces the swimming speed [11] or reduces it for some parameter regimes and increases it for others [10]. In contrast, in the system we study, the volume fractions play a crucial role in that the relative amounts of the more and less viscous fluids strongly affects the swimming speed. In our system, in the limit that one of the volume fractions becomes vanishingly small, the single fluid swimming speed is recovered, but for all other volume fractions, the swimming speed is lower than for a single fluid. For the special case of no friction between the fluids and with the volume fractions held fixed in time, we show that the reduction in swimming speed is by a factor $\mu_{\mathrm{eff}}/\mu_{\mathrm{av}}$, where $\mu_{\mathrm{eff}} = \mu_n \mu_s/(\theta^n \mu_s + \theta^s \mu_n)$ is the volume-fraction-weighted harmonic average of the viscosities μ_n and μ_s of the network and solvent and $\mu_{\mathrm{av}} = \theta^n \mu_n + \theta^s \mu_s$ is the volume-fraction-weighted arithmetic average of the viscosities. This highlights the critical role played by nonzero volume fractions. Further, we show, through novel numerical simulations, that time-dependent spatial variations in the volume fractions also contribute to reducing the swimming speed further.

II. PROBLEM FORMULATION

The problem we study is the flow introduced by propagating transverse waves of small amplitude on an infinite sheet immersed in a viscous two-phase fluid. Similar problems in a

single-phase Stokes fluid were studied by Taylor in an infinite domain [15] and later by Reynolds in a finite domain [16]. In the reference frame moving with its swimming speed, the extensible sheet has a waving profile

$$y = \epsilon \sin(kx - \omega t), \qquad (1)$$

where $\epsilon k \ll 1$. We describe the fluid medium as a mixture composed of two immiscible materials (more viscous network phase labeled as n and less viscous solvent phase labeled as s), with volume fraction of θ^n and θ^s and velocity $\mathbf{u}^n = (u^n, v^n)$ and $\mathbf{u}^s = (u^s, v^s)$, respectively, where $\theta^n + \theta^s = 1$. The system of equations for the velocities and volume fractions is

$$(\theta^n)_t + \nabla \cdot (\theta^n \mathbf{u}^n) = 0, \qquad (2)$$

$$(\theta^s)_t + \nabla \cdot (\theta^s \mathbf{u}^s) = 0, \qquad (3)$$

$$\nabla \cdot (\theta^n \sigma^n) - \beta \theta^n \theta^s (\mathbf{u}^n - \mathbf{u}^s) - \theta^n \nabla p = \mathbf{0}, \qquad (4)$$

$$\nabla \cdot (\theta^s \sigma^s) - \beta \theta^n \theta^s (\mathbf{u}^s - \mathbf{u}^n) - \theta^s \nabla p = \mathbf{0}. \qquad (5)$$

Here σ^n and σ^s are viscous stress tensors and β is the friction constant. The stress in both phases is given by the Newtonian constitutive law,

$$\sigma^{n,s} = \mu_{n,s}(\nabla \mathbf{u}^{n,s} + \nabla \mathbf{u}^{n,s\,T}) + (\lambda_{n,s} \nabla \cdot \mathbf{u}^{n,s})\delta, \qquad (6)$$

where $\mu_{n,s}$ and $\lambda_{n,s}$ are first and second viscosity coefficients and δ is the identity tensor. In this paper we set $\lambda_{n,s} = -\mu_{n,s}$. From Eqs. (2) and (3) we obtain the incompressibility condition for the mixture,

$$\nabla \cdot (\theta^n \mathbf{u}^n + \theta^s \mathbf{u}^s) = 0. \qquad (7)$$

No-slip boundary conditions are satisfied by both $\mathbf{u}^n$ and $\mathbf{u}^s$ on the sheet.

III. NUMERICAL METHOD

We use the numerical method introduced in Ref. [17] to solve the fluid equations. Given a distribution of network volume fraction, the method uses the generalized minimal residual method (GMRES) with a box-type multigrid scheme preconditioner to solve collectively the momentum and incompressibility equations (4), (5), and (7) to get $\mathbf{u}^n$, $\mathbf{u}^s$, and p. Then θ^n is updated by solving the transport equation (2) using a high-resolution unsplit Godunov scheme as described in Ref. [18]. All simulations were done in the laboratory frame.

To capture the coupled fluid-structure interactions between the swimmer and the surrounding fluid mixture, we develop an extension of the classical immersed boundary method [14]. Because of the existence of two velocity fields, we represent the sheet by two immersed boundaries, denoted Γ^n and Γ^s as illustrated in Fig. 1. Each of the immersed boundaries is composed of an array of discrete Lagrangian points connected by linear springs and communicates with only one of the fluids in the mixture. That is, forces from Γ^n are spread only to fluid n, and values of $\mathbf{u}^n$ are interpolated to points of Γ^n to update their positions. Similarly, Γ^s interacts with fluid s. Each immersed boundary point on each of Γ^n or Γ^s is connected with its neighboring points by weak springs in order to simulate an extensible sheet. The up and down motions of the immersed boundary points are driven by linking them to moving "tether" points through stiff springs with zero rest
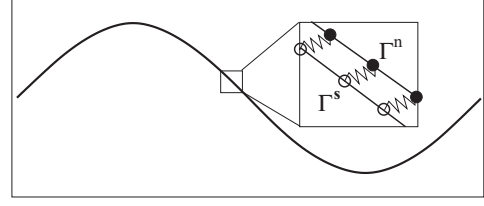
FIG. 1. IB representation of the swimming sheet.

length. The y coordinate of each tether point moves according to $y = \epsilon \sin(kx_0 - \omega t)$, where x_0 is its initial x coordinate. The springs to the tether points generate forces in the y direction only. Penalty forces are introduced by adding stiff springs between corresponding points on Γ^s and Γ^n. Each penalty spring generates a force in the x direction whenever the x coordinates of the points it connects differ. After the usual immersed boundary spreading of forces to the Eulerian grid used for the fluid dynamics variables, the spread contributions from the penalty forces are scaled with the product of the two volume fractions to ensure that there are no interphase forces whenever one of the volume fractions goes to zero. Spread contributions from forces within each phase are scaled with the volume fraction of that phase. We denote the penalty force by $F_p^{n,s}$, and the force from the springs to tether points and neighboring immersed boundary points by $F_o^{n,s}$. In the immersed boundary framework, Eqs. (4) and (5) have the form,

$$\nabla \cdot (\theta^n \sigma^n) - \beta \theta^n \theta^s (\mathbf{u}^n - \mathbf{u}^s) - \theta^n \nabla p + \mathbf{f}^n = \mathbf{0}, \quad (8)$$

$$\nabla \cdot (\theta^s \sigma^s) - \beta \theta^n \theta^s (\mathbf{u}^s - \mathbf{u}^n) - \theta^s \nabla p + \mathbf{f}^s = \mathbf{0}, \quad (9)$$

where $\mathbf{f}^{n,s} = \theta^{n,s} S(F_o^{n,s}) + \theta^n \theta^s S(F_p^{n,s})$. S is the standard force spreading operator for the immersed boundary method [14] and $F_p^n = -F_p^s$.

IV. SIMULATION RESULTS

Our numerical simulations are carried out in the domain $[0,1] \times [-L, L]$, where L is the distance from the mean plane of the waving sheet to the top wall. The boundary condition in the x direction is periodic and that at $y = \pm L$ is no-slip. Initially θ^n is set to the same constant value everywhere. The swimming speed is calculated by averaging the x velocity over all the immersed boundary points and over one wave period. For the results presented in this paper, we use $\epsilon = 0.012$ and
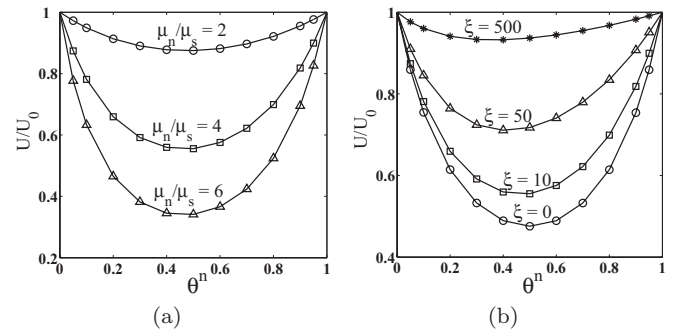
FIG. 2. (a) Scaled swimming speed as a function of the initial θ^n for various values of μ_n/μ_s, with $\xi = 40$. (b) Scaled swimming speed as a function of the initial θ^n for various values of ξ, with $\mu_n/\mu_s = 4$.

(a) network velocity   (b) solvent velocity
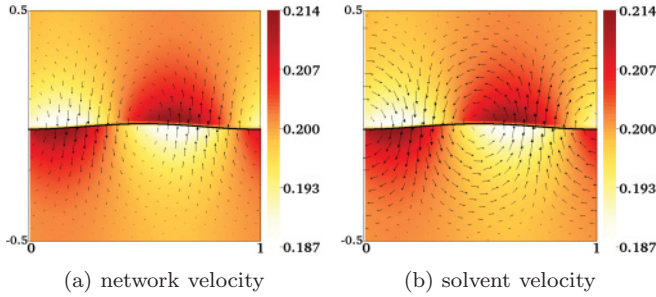
FIG. 3. (Color online) Color field of θ^n distribution along with the vector fields of $\mathbf{u}^n$ and $\mathbf{u}^s$. $\theta^n(t=0) = 0.2, \xi = 0$ and $\mu_n/\mu_s = 4$. $||\mathbf{u}^n||_{\max} = ||\mathbf{u}^s||_{\max} = 0.076$.

$k = \omega = 2\pi$. $L = 0.5$ unless stated otherwise. A 256×256 grid is used for a unit square computational domain. Our tests show the results are essentially unchanged on finer grids. We define a dimensionless friction constant $\xi = \lambda^2 \beta/\mu_n$, where $\lambda = 2\pi/k$ is the wavelength. ξ measures the magnitude of the friction force relative to the network viscous force.

First, setting $\mu_n = \mu_s$, we get a numerical swimming speed of $U = 3.2 \times 10^{-3}$, which agrees well with the analytic speed $U_0 = 3.3 \times 10^{-3} + O(\epsilon^4)$ in a single fluid [16]. We next test different parameter values with $\mu_n \neq \mu_s$ to see how the swimming speed is affected. Figure 2(a) shows, for fixed friction constant $\xi = 40$, the ratio of the swimming speed in the mixture to that in a single fluid U/U_0 as a function of initial θ^n values for different viscosity ratios. The plot indicates that the sheet always swims more slowly in the mixture than in a single fluid. The swimming speed decreases as the viscosity ratio increases. In Fig. 2(b), we see that for a fixed viscosity ratio and different values of the friction constant ξ, the scaled swimming speed remains less than 1, and that it increases with ξ. For each value of ξ, the swimming speed is minimized for a value of $\theta^n \in (0, 1/2)$, so increases in the volume fraction of the more viscous phase can cause slowing or speeding of the swimming. The location of the minimum approaches $\theta^n = 1/2$ as $\xi \to 0$.

Figure 3 shows θ^n and the two velocity fields at $t = 0.25$ from a simulation, with the friction constant ξ set to zero. There is a significant difference between $\mathbf{u}^n$ and $\mathbf{u}^s$ and spatial inhomogeneities of θ^n have developed. Even with no friction between the fluids, the two fluids are coupled through the incompressibility condition (7) and this condition determines a single pressure field felt by both fluids. Figure 4 shows θ^n

(a)   (b)
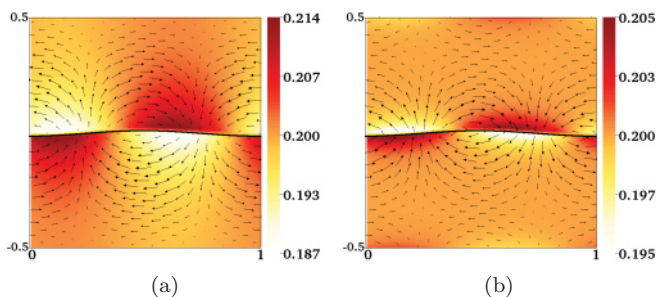
FIG. 4. (Color online) $\mu_n/\mu_s = 4$. Color field of θ^n distribution along with the vector field of the relative velocity $\mathbf{u}^n - \mathbf{u}^s$. $\theta^n(t = 0) = 0.2$. (a) $\xi = 0$ and $||\mathbf{u}^n - \mathbf{u}^s||_{\max} = 0.033$ (b) $\xi = 500$ and $||\mathbf{u}^n - \mathbf{u}^s||_{\max} = 0.005$.
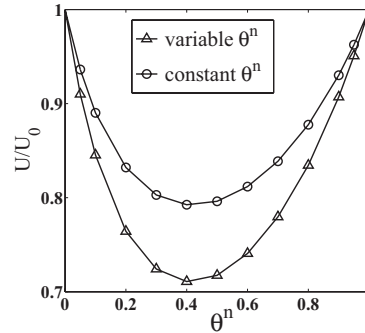
FIG. 5. Scaled swimming speed from simulations with spatially uniform and variable network volume fractions, with $\mu_n/\mu_s = 4$ and $\xi = 50$.

and the relative velocity $\mathbf{u}^n - \mathbf{u}^s$ distributions from simulations with $\xi = 0$ and $\xi = 500$. The distribution of $\mathbf{u}^n - \mathbf{u}^s$ is consistent with the phase separation. It is also clear that with a large friction constant, the two fluids tend to move together and, thus, both the θ^n inhomogeneities and magnitude of the relative velocity are greatly reduced. Our simulation results suggest that $U/U_0 \to 1$ as the friction constant increases or the viscosity ratio μ_n/μ_s approaches 1. As shown in the analysis below, U/U_0 indeed does go to 1 in these cases because, in both of these limits, the fluid mixture behaves more and more like a single fluid.

We thought initially that the slower swimming was due to the development of nonuniform distributions of θ^n. In order to test this, we also carried out simulations in which θ^n and θ^s were held at their spatially uniform initial values for all time. This can be thought of as the effect of introducing large diffusion terms in Eqs. (2) and (3). Figure 5 shows a comparison between the scaled swimming speeds in two sets of simulations that differed only in whether θ^n changed according to Eq. (2) or was held fixed in time. In both cases the swimming speed in the mixture is smaller than the speed in a single viscous fluid. The dependence of the swimming speed on θ^n is similar, but the swimming speed is significantly slower when θ^n evolves according to Eq. (2). Thus the phase separation has a significant effect, but even without phase separation, the swimmer moves more slowly in the mixture than in a single fluid.

V. ANALYSIS: INFINITE DOMAIN AND WITH FRICTION

As shown above, the swimming speeds in the variable and spatially uniform θ^n cases have similar profiles. To simplify the analytical study of the problem, we solve the boundary value problem of Eqs. (4), (5), and (7) for $\mathbf{u}^n$, $\mathbf{u}^s$, and p with spatially uniform volume fractions. The domain is infinite in both the x and y directions. We also assume that the sheet is freely extensible and that it swims at an unknown speed U. From the no-slip boundary conditions, in the reference frame of the swimmer,

$$u^j(x, \epsilon \sin(kx - \omega t)) = 0, \qquad (10)$$

$$v^j(x, \epsilon \sin(kx - \omega t)) = -\epsilon \omega \cos(kx - \omega t), \qquad (11)$$

where $j = n, s$. To solve the problem, we use eigenfunction expansions for the system in powers of ϵ and solve the
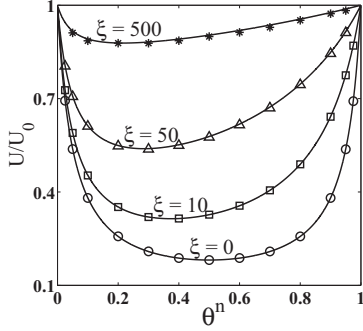
FIG. 6. Comparison of the swimming speed from numerical simulation ($\bigcirc$, $\square$, $\triangle$, and $*$) and analysis (curves). $\mu_n/\mu_s = 20$.

equations order by order. (See the Appendix for details.) The swimming speed is the opposite of the fluid velocity at infinity. After some calculations, we find that to order ϵ^2, the swimming speed is

$$U = -\frac{\epsilon^2 \omega k}{2}\frac{G-1}{G+1} \equiv U_0 \frac{G-1}{G+1}, \qquad (12)$$

where

$$G = \frac{\beta(\mu_n \theta^n + \mu_s \theta^s)(\kappa_1 \kappa_2 - 1)}{2k^2 \theta^n \theta^s (\mu_n - \mu_s)^2(\kappa_1 - 1)(\kappa_2 - 1)}, \qquad (13)$$

with $\kappa_1^2 = 1 + \frac{\beta}{k^2(\mu_n\theta^s + \mu_s\theta^n)}$ and $\kappa_2^2 = 1 + \frac{\beta(\mu_n\theta^n + \mu_s\theta^s)}{k^2\mu_n\mu_s}$. $U_0 = -\epsilon^2\omega k/2$ is the classical result given in Ref. [15] for a single fluid. Note that as friction constant $\beta \to \infty$, $(G-1)/(G+1) \to 1$ and $U \to U_0$. Taking the limit of Eq. (12) as $\beta \to 0$, we have

$$U(\beta = 0) = U_0 \frac{\mu_n \mu_s}{(\theta^n \mu_s + \theta^s \mu_n)(\theta^n \mu_n + \theta^s \mu_s)}. \qquad (14)$$

Figure 6 compares the analytical scaled swimming speed $U/U_0 = (G-1)/(G+1)$ with the results from numerical simulations with θ^n held constant for a number of values of the friction constant ξ. In the simulations, the boundary position L is set to a value sufficiently large that the swimming speed is essentially independent of it. The match is excellent.

VI. ANALYSIS: FINITE DOMAIN AND WITHOUT FRICTION

Next we adopt a different strategy in the solution procedure to get some physical insights into the reason the sheet always swims more slowly in a two-fluid mixture. To simplify the analysis, we also assume that $\beta = 0$, since from previous results, the frictionless case always has the most significant reduction of the swimming speed. For a Stokes swimmer, the swimming speed is determined by a balance of thrust and drag forces [3]. Here the thrust is defined as the anchoring force applied so that the undulating sheet is prevented from swimming and the drag is the force required to tow the sheet at speed U with a frozen shape. In order to apply the force balance condition, we put the infinite swimming sheet at the center of a channel, with rigid walls at $y = \pm L$. The analysis is limited to the fluid domain above the sheet.

First, to find the thrust, we solve the boundary value problem [Eqs. (4), (5), and (7)] in the laboratory frame (which is also the swimming frame since the swimming speed in this

case is zero) with spatially uniform volume fractions, subject to the boundary conditions

$$u^j(x,\epsilon \sin(kx - \omega t)) = 0, \qquad (15)$$

$$v^j(x,\epsilon \sin(kx - \omega t)) = -\epsilon\omega\cos(kx - \omega t), \qquad (16)$$

$$\mathbf{u}^j(x,L) = \mathbf{0}, \qquad (17)$$

where $j = n,s$. Defining the volume-fraction averaged velocity $\mathbf{u}^{\mathrm{av}} = \theta^n \mathbf{u}^n + \theta^s \mathbf{u}^s$, multiplying Eq. (4) by μ_s and Eq. (5) by μ_n, and then adding the two, we get

$$\mu_{\mathrm{eff}} \Delta \mathbf{u}^{\mathrm{av}} - \nabla p = \mathbf{0} \quad \text{and} \quad \nabla \cdot \mathbf{u}^{\mathrm{av}} = 0. \qquad (18)$$

The effective viscosity of the mixture μ_{eff} is defined by

$$\mu_{\mathrm{eff}} = \frac{\mu_n \mu_s}{\theta^n \mu_s + \theta^s \mu_n}. \qquad (19)$$

We first solve Eq. (18) subject to the boundary conditions of Eqs. (15)–(17) to find the pressure p and then solve the Poisson equations (4) and (5) for the individual velocities $\mathbf{u}^n$ and $\mathbf{u}^s$. To order ϵ^2, we find that the horizontal component of the force (averaged over a wave period $2\pi/\omega$ and a wavelength) exerted by fluid j on the upper surface of the sheet is $-\theta^j \epsilon^2 \mu_{\mathrm{eff}} \omega k C(kL)/(2L)$, where $C(Z) = [\sinh^2(Z) + Z^2]/[\sinh^2(Z) - Z^2]$. It follows that the total anchoring force on the sheet (the thrust) is

$$F_T = \epsilon^2 \mu_{\mathrm{eff}} \omega k \frac{C(kL)}{2L}. \qquad (20)$$

Note that this is also the thrust generated in a single-phase fluid whose viscosity has value μ_{eff}.

To find the drag, we solve the same set of equations as above. In the reference frame of the sheet moving with speed U, the boundary conditions are

$$u^j(x,\epsilon \sin(kx)) = 0, \qquad (21)$$

$$v^j(x,\epsilon \sin(kx)) = 0, \qquad (22)$$

$$u^j(x,L) = -U, \qquad (23)$$

$$v^j(x,L) = 0, \qquad (24)$$

for $j = n,s$. Using a similar solution procedure, we find that, to leading order in ϵ, dragging the sheet induces a simple shear flow for both fluids and $\mathbf{u}^n(x,y) = \mathbf{u}^s(x,y) = (-Uy/L,0)$. The horizontal component of the force on the upper surface of the sheet from fluid j then is $-\theta^j \mu_j U/L$, and the total drag force on the sheet is

$$F_D(U) = (\theta^n \mu_n + \theta^s \mu_s)\frac{U}{L} \equiv \mu_{\mathrm{av}}\frac{U}{L}, \qquad (25)$$

where

$$\mu_{\mathrm{av}} = \theta^n \mu_n + \theta^s \mu_s \qquad (26)$$

is the volume-fraction averaged viscosity. Requiring that the sum of the thrust and drag be zero, we find the swimming speed

$$U = -\frac{1}{2}\epsilon^2 \omega k C(kL)\frac{\mu_{\mathrm{eff}}}{\mu_{\mathrm{av}}} = \frac{\mu_{\mathrm{eff}}}{\mu_{\mathrm{av}}}U_0, \qquad (27)$$

where $U_0 = -\epsilon^2\omega k C(kL)/2$ is the swimming speed given by Ref. [16] for a single fluid. Notice that $C(kL) \to 1$ as $L \to \infty$

and, from the definitions of μ_{eff} and μ_{av}, Eq. (27) is consistent with the previous result for an infinite domain (14). From the definitions of μ_{eff} and μ_{av}, the speed ratio is given by

$$\frac{U}{U_0} = \frac{\mu_{\text{eff}}}{\mu_{\text{av}}} = \frac{1}{\left(\frac{\mu_n}{\mu_s} + \frac{\mu_s}{\mu_n} - 2\right)\left[\frac{1}{4} - \left(\theta^n - \frac{1}{2}\right)^2\right] + 1}. \quad (28)$$

Several conclusions follow directly:

(i) When $\mu_n = \mu_s$, or $\theta^n = 0$ or 1, $\mu_{\text{eff}}/\mu_{\text{av}} = 1$. That is, the mixture essentially contains only one phase of fluid and the results in Ref. [16] are recovered.

(ii) When $\mu_n \neq \mu_s$, and θ^n is other than 0 or 1, $\mu_{\text{eff}}/\mu_{\text{av}} < 1$ and $U < U_0$. Thus, the swimming speed in a mixture is always less than that in a single fluid.

(iii) With fixed θ^n, the swimming speed decreases with increasing viscosity ratio μ_n/μ_s.

(iv) With fixed viscosity ratio μ_n/μ_s, the minimum swimming speed is achieved at $\theta^n = 1/2$.

All these findings are consistent with numerical experiments.

The hydrodynamic efficiency is defined as the ratio of the power required to drag the swimmer with a frozen shape at speed U to the average rate of work done by the swimmer [3]. From the solutions given above, the efficiency of the swimming sheet is found to be

$$\eta = \frac{\mu_{\text{eff}}}{\mu_{\text{av}}} D \frac{k\epsilon^2}{4L} = \frac{\mu_{\text{eff}}}{\mu_{\text{av}}} \eta_0, \quad (29)$$

where $D = \frac{[\sinh^2(kL)+k^2L^2]^2}{[\sinh^2(kL)-k^2L^2][\cosh(kL)\sinh(kL)+kL]}$ and $\eta_0 = Dk\epsilon^2/(4L)$ is the corresponding single fluid efficiency. Thus, swimming in a two-fluid mixture is less efficient than in a single fluid.

From Eq. (25), we define the drag coefficient as $\gamma = F_D(1)$. The swimming speed then is given by $U = -F_T/\gamma$. In Fig. 7, we plot the thrust force and drag coefficient from numerical simulations with spatially uniform θ^n. We also plot the analytical solutions given by Eqs. (20) and (25), multiplied by a factor of 2 since the analysis is limited to the fluid domain above the sheet. It is clear that simulations with $\xi = 0$ give thrust forces and drag coefficients in good agreement with the analytical results. The plot shows that the drag coefficient is
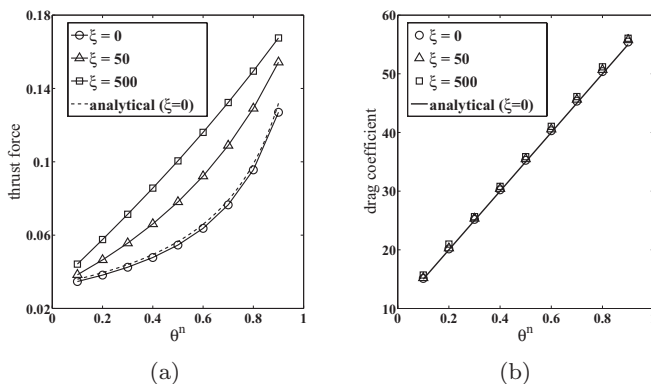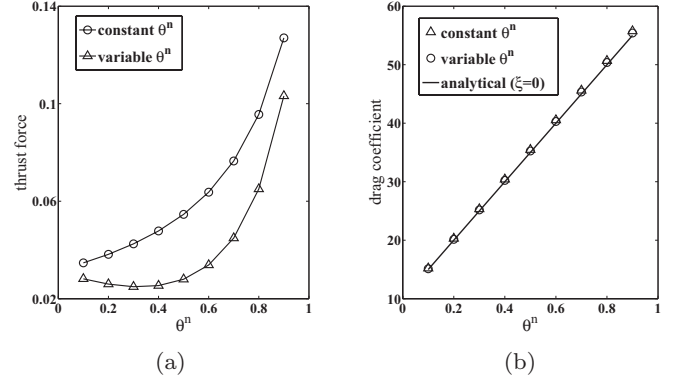
FIG. 8. $\mu_n = 15$, $\mu_s = 2.5$, $\xi = 0$, and $L = 0.5$. (a) Thrust force for constant and variable θ^n. (b) Drag coefficient for constant and variable θ^n.

insensitive to the friction constant. It is proportional to μ_{av} and, thus, a linear function of θ^n. The thrust force is a strictly convex function of θ^n; it is always less than the thrust generated in a single-phase medium with viscosity μ_{av}. With other conditions the same, swimming in a fluid mixture with a larger friction constant can generate a larger thrust force.

Figure 8 compares the thrust force and drag coefficient from two sets of simulations that differed only in whether θ^n was allowed to vary or was held fixed in time. Figure 8(b) indicates that even when θ^n is allowed to change, the numerical drag forces agree well with Eq. (25). In the simulations used to calculate the numerical drag, only small pressure gradients develop, and the two velocities $\mathbf{u}^n$ and $\mathbf{u}^s$ remain very close, and so, in fact, θ^n changes little. As shown in Fig. 8(a), the thrust force from variable θ^n simulations is smaller than that from constant θ^n simulations, which leads to a smaller swimming speed as indicated by Fig. 5.

VII. DISCUSSION

In a single Newtonian fluid, the speed of translation for Taylor's swimming sheet is independent of the fluid viscosity. This is because both the thrust force generated by the sheet and the drag force exerted on it by the fluid are proportional to the single viscosity. The results presented in this paper show that the swimming speed of the sheet in a two-fluid mixture depends on the viscosities of both fluids and the compositions of the mixture. Numerical simulations show that the swimming speed in a mixture of two fluids with different viscosities is always less than that of a single fluid. From the simulation results, we see that the drag force increases linearly with the volume fraction of the more viscous fluid, while the thrust varies in a more complex way as the volume fractions change. We obtained insight into the origin of this behavior by analyzing the special case in which there is no friction between the two fluids, and the volume fractions were held fixed in time. That analysis shows that the drag force scales with $\mu_{\text{av}} = \theta^n \mu_n + \theta^s \mu_s$, while the thrust force scales with $\mu_{\text{eff}} = \mu_n \mu_s/(\theta^n \mu_s + \theta^s \mu_n)$, and that the swimming speed in the mixture equals the single fluid swimming speed multiplied by the ratio $\mu_{\text{eff}}/\mu_{\text{av}}$, which is always less than 1. Because

FIG. 7. $\mu_n = 15$, $\mu_s = 2.5$, and $L = 0.5$, spatially uniform θ^n. (a) Thrust force as a function of the initial θ^n for various values of ξ. (b) Drag coefficient as a function of the initial θ^n for various values of ξ.

of the different dependence of these two viscosities on the volume fractions of the mixture, the swimming speed is also a function of these volume fractions, as well as the individual viscosities of the two fluids. Comparison of numerical results from simulations of this special case and of the case in which the volume fractions evolved according to the appropriate continuity equations shows that the swimming speed is further reduced when spatial variations in the volume fraction are allowed to develop.

Research on swimming in two-fluid media is just beginning, and early theoretical works have yielded some surprising results. For example, the infinite swimmer is slowed by elastic stresses in a single-phase fluid [5,6], but relative motion between the swimmer and the elastic phase may increase the swimming speed [10,11]. For a given deformation, swimming in a single-phase viscous fluid is independent of the viscosity, but as we have shown here, in a mixture of two viscous fluids, the swimming speed depends on the viscosities. Numerical simulations are essential to fully explore more realistic problems of locomotion in complex biological fluids. Including effects such as swimmers of finite length, large-amplitude deformations, and nonuniform network concentrations is straightforward with our numerical method, and it can be readily adapted to include different rheological properties for the network, as well as more general network boundary conditions on the swimmer surface, and is the subject of ongoing work.

ACKNOWLEDGEMENT

APPENDIX

In this Appendix, we provide additional details of the analytical solutions described above. Two of the problems we solve have time-dependent boundary conditions, but because the partial differential equations are independent of time, the force averaged over a wavelength and swimming speeds are independent of time as well. As formulated in Secs. V and VI, all the problems we solve have boundary conditions of the form

$$u^j(x, \epsilon \sin(kx)) = 0, \tag{A1}$$

$$v^j(x, \epsilon \sin(kx)) = -\epsilon \omega \cos(kx), \tag{A2}$$

$$u^j(x, L) = -u_0, \tag{A3}$$

$$v^j(x, L) = 0, \tag{A4}$$

with different values of ω, u_0, or L. Here $j = n, s$. To solve these problems we use perturbation methods, seeking solutions as power series in ϵ of the form,

$$\mathbf{u}^j = \epsilon \mathbf{u}_1^j + \epsilon^2 \mathbf{u}_2^j + \cdots. \tag{A5}$$

Expanding the boundary conditions in powers of ϵ, we find the requirements

$$u_1^j(x, 0) = 0, \quad v_1^j(x, 0) = -\omega \cos(kx), \tag{A6}$$

$$u_2^j(x, 0) = -\sin(kx)\frac{\partial u_1^j}{\partial y}(x, 0),$$

$$v_2^j(x, 0) = -\sin(kx)\frac{\partial v_1^j}{\partial y}(x, 0). \tag{A7}$$

In the discussions below, we assume θ^n and θ^s are spatially uniform constants and take $\lambda_{n,s} = -\mu_{n,s}$.

1. Infinite domain with friction

In the case that the domain is infinite ($L = \infty$), our goal is to find the quantity

$$\mathbf{V} = \begin{pmatrix} u^n \\ v^n \\ u^s \\ v^s \\ p \end{pmatrix}, \tag{A8}$$

which satisfies the equations

$$\mu_n \theta^n \Delta \mathbf{u}^n - \beta \theta^n \theta^s (\mathbf{u}^n - \mathbf{u}^s) - \theta^n \nabla p = \mathbf{0}, \tag{A9}$$

$$\mu_s \theta^s \Delta \mathbf{u}^s - \beta \theta^n \theta^s (\mathbf{u}^s - \mathbf{u}^n) - \theta^s \nabla p = \mathbf{0}, \tag{A10}$$

$$\nabla \cdot (\theta^n \mathbf{u}^n + \theta^s \mathbf{u}^s) = 0, \tag{A11}$$

with θ^n and θ^s constant, subject to the boundary conditions of Eqs. (A1) and (A2), with the additional restriction that the solution is bounded in the limit $y \to \infty$. For this problem, the swimming speed is the $-u^{n,s}(x, y \to \infty)$.

The solution is formed as the superposition of eigenfunctions,

$$\phi_1(x, y) = \begin{pmatrix} \sin x \\ \cos x \\ \sin x \\ \cos x \\ 0 \end{pmatrix} e^{-y}, \tag{A12}$$

$$\phi_2(x, y) = \begin{pmatrix} \left[-2d\mu + \frac{\beta}{k^2}(-1 + 2y)\right]\sin x \\ \left[-2d\mu + \frac{\beta}{k^2}(1 + y)\right]\cos x \\ \left[2d\mu + \frac{\beta}{k^2}(-1 + 2y)\right]\sin x \\ \left[2d\mu + \frac{\beta}{k^2}(1 + 2y)\right]\cos x \\ 4\frac{\beta}{k^2}(\mu_n \theta^n + \mu_s \theta^s)\cos x \end{pmatrix} e^{-y}, \tag{A13}$$

$$\phi_3(x, y) = \begin{pmatrix} -\theta^n \sin x \\ -\kappa_1 \theta^s \cos x \\ \theta^n \sin x \\ \kappa_1 \theta^n \cos x \\ \frac{\beta}{k^2}\frac{d\mu\theta^s\theta^n}{(\theta^n \mu_s + \theta^s \mu_n)}\cos x \end{pmatrix} e^{-\kappa_1 y}, \tag{A14}$$

$$\phi_4(x, y) = \begin{pmatrix} -\kappa_2 \mu_s \theta^s \sin x \\ -\mu_s \theta^s \cos x \\ \kappa_2 \mu_n \theta^n \sin x \\ \mu_n \theta^n \cos x \\ 0 \end{pmatrix} e^{-\kappa_2 y}, \tag{A15}$$

where

$$\kappa_1^2 = 1 + \frac{\beta}{k^2}\frac{1}{(\mu_n\theta^s + \theta^n\mu_s)}, \quad \kappa_2^2 = 1 + \frac{\beta}{k^2}\frac{(\mu_n\theta^n + \theta^s\mu_s)}{\mu_n\mu_s},$$
$$\text{(A16)}$$

and $d\mu = \mu_n - \mu_s$. In addition, there are solutions independent of x of the form

$$\phi_5(y) = \begin{pmatrix} \theta^s\mu_s \\ 0 \\ -\theta^n\mu_n \\ 0 \\ 0 \end{pmatrix} e^{-\kappa_s y} \qquad \text{(A17)}$$

$$\phi_6(y) = \begin{pmatrix} 1 \\ 0 \\ 1 \\ 0 \\ 0 \end{pmatrix}, \qquad \text{(A18)}$$

where $\kappa_s = \beta\frac{\mu_s\theta^s + \mu_n\theta^n}{\mu_n\mu_s}$.

The solution then takes the form

$$\mathbf{V} = \epsilon\sum_{i=1}^{4} a_i\phi_i(kx,ky) + \epsilon^2\sum_{i=1}^{4} b_i\phi_i(2kx,2ky)$$
$$+ \epsilon^2 b_5\phi_5(y) + U\phi_6. \qquad \text{(A19)}$$

Following an extended calculation in which the coefficients are determined so the boundary conditions are satisfied, we find the swimming speed U as reported in Eq. (12).

2. Finite domain without friction

To find the thrust, we solve the boundary value problem,

$$\mu_n\theta^n\Delta\mathbf{u}^n - \theta^n\boldsymbol{\nabla}p = \mathbf{0}, \qquad \text{(A20)}$$
$$\mu_s\theta^s\Delta\mathbf{u}^s - \theta^s\boldsymbol{\nabla}p = \mathbf{0}, \qquad \text{(A21)}$$
$$\boldsymbol{\nabla}\cdot(\theta^n\mathbf{u}^n + \theta^s\mathbf{u}^s) = 0, \qquad \text{(A22)}$$

subject to the boundary conditions [Eqs. (A1)–(A4)] with $u_0 = 0$.

We solve this as follows. First, setting $\mathbf{u}^{av} = \theta^n\mathbf{u}^n + \theta^s\mathbf{u}^s$ and $\mathbf{u}^{av} = (u^{av}, v^{av})$, we find

$$\mu_{\text{eff}}\Delta\mathbf{u}^{av} - \boldsymbol{\nabla}p = \mathbf{0}, \qquad \text{(A23)}$$

where $\mu_{\text{eff}} = \frac{\mu_n\mu_s}{\theta^n\mu_s + \theta^s\mu_n}$. We set $u^{av} = \frac{\partial\psi}{\partial y}$ and $v^{av} = -\frac{\partial\psi}{\partial x}$, so ψ satisfies the biharmonic equation $\nabla^4\psi = 0$. We solve this to find the pressure p and then solve the Poisson equations (A20) and (A21) for the individual velocities.

To solve the biharmonic equation, we take $\psi = \epsilon\psi_1 + \epsilon^2\psi_2$, where

$$\psi_1 = [(a_0 y + b_0)e^{ky} + (c_0 y + d_0)e^{-ky}]\sin(kx) \quad \text{(A24)}$$

and

$$\psi_2 = [(a_1 y + b_1)e^{2ky} + (c_1 y + d_1)e^{-2ky}]\cos(2kx)$$
$$+ s_1 y(2L - y). \qquad \text{(A25)}$$

From this we find

$$p = -2\epsilon\mu_{\text{eff}}(a_0 e^y + c_0 e^{-ky})\cos(kx)$$
$$+ 4\epsilon^2\mu_{\text{eff}}(a_1 e^{2ky} + c_1 e^{-2ky})\sin(2kx). \quad \text{(A26)}$$

Then, for each of Eqs. (A20) and (A21), we set

$$u_1 = [(A_0 y + B_0)e^{ky} + (C_0 y + D_0)e^{-ky}]\sin(kx), \quad \text{(A27)}$$
$$v_1 = [(A_1 y + B_1)e^{ky} + (C_1 y + D_1)e^{-ky}]\cos(kx), \quad \text{(A28)}$$

and

$$u_2 = [(A_3 y + B_3)e^{2ky} + (C_3 y + D_3)e^{-2ky}]\cos(2kx)$$
$$+ \frac{S_2}{\mu_j}(y - L), \qquad \text{(A29)}$$

$$v_2 = [(A_4 y + B_4)e^{2ky} + (C_4 y + D_4)e^{-2ky}]\sin(2kx). \quad \text{(A30)}$$

The spatially averaged value of the total shear force on the wall at $y = L$ is $\epsilon^2 S_2$, which, after an extended calculation, we find to be

$$S_2 = \frac{\mu_{\text{eff}}\omega k}{2L}C(kL), \qquad \text{(A31)}$$

where

$$C(L) = \frac{\sinh^2(L) + L^2}{\sinh^2(L) - L^2}. \qquad \text{(A32)}$$

By the divergence theorem, the horizontal component of the force exerted on the sheet by the fluids is $-\epsilon^2 S_2$. It follows that the thrust force must be $\epsilon^2 S_2$ to satisfy the force balance condition on the sheet, namely

$$F_T = \epsilon^2\mu_{\text{eff}}\omega k\frac{C(kL)}{2L}. \qquad \text{(A33)}$$

The second problem is to find the drag. This is found by solving the partial differential equations (A20)–(A22) subject to the boundary conditions [Eqs. (A1)–(A4)] with $\omega = 0$. For this problem the solution of the biharmonic equation takes the form $\psi = \psi_0 + \epsilon\psi_1 + \cdots$, where

$$\psi_0 = -\frac{u_0}{2}\frac{y^2}{L} \qquad \text{(A34)}$$

and the individual velocities are

$$u_0^j = -u_0\frac{y}{L}, \quad v_0^j = 0, \qquad \text{(A35)}$$

where $j = n,s$. Thus the shear force exerted on the sheet by fluid j with volume fraction θ^j is $-\frac{\mu_j u_0}{L}\theta^j$. Since the drag force required to pull the sheet with speed u_0 has to balance the total shear force, we have

$$F_D = (\theta^n\mu_n + \theta^s\mu_s)\frac{u_0}{L}. \qquad \text{(A36)}$$

[1] H. Berg, *E. Coli in Motion* (Springer, New York, 2004).

[2] L. Fauci and R. Dillon, Annu. Rev. Fluid Mech. **38**, 371 (2006).

[3] E. Lauga and T. Powers, Rep. Prog. Phys. **72**, 096601 (2009).

[4] T. Normand and E. Lauga, Phys. Rev. E **78**, 061907 (2008).

[5] E. Lauga, Phys. Fluids **19**, 083104 (2007).

[6] H. C. Fu, T. R. Powers, and C. W. Wolgemuth, Phys. Rev. Lett. **99**, 258101 (2007).

[7] E. Lauga, Europhys. Lett. **86**, 64001 (2009).

[8] A. M. Leshansky, Phys. Rev. E **80**, 051911 (2009).

[9] J. Teran, L. Fauci, and M. Shelley, Phys. Rev. Lett. **104**, 038101 (2010).

[10] H. Fu, V. Shenoy, and T. Powers, Europhys. Lett. **91**, 24002 (2010).

[11] H. Wada, e-print arXiv:1004.1254v1 (2010).

[12] M. Doi, J. Phys. Soc. Jpn. **78**, 052001 (2009).

[13] N. Cogan and R. Guy, HFSP J **4**, 11 (2010).

[14] C. Peskin, Acta Numer. **11**, 479 (2002).

[15] G. I. Taylor, Proc. R. Soc. A **209**, 447 (1951).

[16] A. J. Reynolds, J. Fluid Mech. **23**, 241 (1965).

[17] G. Wright, R. Guy, and A. Fogelson, SIAM J. Sci. Comput. **30**, 2535 (2008).

[18] P. Colella, J. Comput. Phys. **87**, 171 (1990).